EUROPEAN ORGANIZATION FOR NUCLEAR RESEARCH

p̄p ANNIHILATION INTO $\pi^+\pi^-$ and K^+K^- FROM ATOMIC p STATES

ASTERIX COLLABORATION

M. Doser[1], M. Botlo[2a], S. Ahmad[3b], C. Amsler[1], R. Armenteros[4],
E.G. Auld[5], D.A. Axen[5], D. Bailey[4c], S. Barlag[4d], G.A. Beer[6],
J.C. Bizot[3], J. Butler[4], M. Comyn[7], W. Dahme[8e], B. Delcourt[3],
K.D. Duch[9], K.L. Erdman[5], F. Feld−Dahme[8], U. Gastaldi[4], M. Heel[9f],
B. Howard[5], R. Howard[5], J. Jeanjean[3], H. Kalinowsky[9], F. Kayser[9g],
E. Klempt[9], C. Laa[2], R. Landua[4], G.M. Marshall[6], B. May[9], H. Nguyen[3],
N. Prevot[3], J. Riedlberger[1], L.P. Robertson[6], C. Sabev[h],
U. Schaefer[8i], O. Schreiber[9j], U. Straumann[1], P. Truöl[1],
H. Vonach[2], B.L. White[5], R.W. Wodrich[8k] and M. Ziegler[9].

1) University of Zürich, Switzerland
2) University of Vienna, Austria
3) LAL, Orsay, France
4) CERN, Geneva, Switzerland
5) University of British Columbia, Vancouver, Canada
6) University of Victoria, Canada
7) TRIUMF, Vancouver, Canada
8) University of Munich, Fed. Rep. Germany
9) University of Mainz, Fed. Rep. Germany

a) present address: Austrian Academy of Science, Vienna, Austria.
b) present address: TRIUMF, Vancouver, Canada.
c) present address: University of Toronto, Canada.
d) present address: Max Planck Institut, Munich, Fed. Rep. Germany.
e) present address: LeCroy Research Systems, Geneva, Switzerland.
f) present address: Boehringer, Ingelheim, Fed. Rep. Germany
g) present address: Volkshochschule, Hanau, Fed. Rep. Germany.
h) visitor at CERN, Geneva, Switzerland.
i) present address: DVFLR, Stuttgart. Fed. Rep. Germany.
j) present address: Siemens, Munich, Fed. Rep. Germany.
k) present address: Schott Glaswerke, Mainz, Fed. Rep. Germany.

ABSTRACT

We have obtained the branching ratios for $\bar{p}p$ annihilation at rest into $\pi^+\pi^-$ and K^+K^- in a pure $\bar{p}p$ initial angular momentum state $L=1$. A gaseous hydrogen target at normal pressure and temperature was used and events associated with transitions of the antiprotonic atom to the 2p level were selected by detecting the Balmer $X-$ray series. The branching ratios for $\bar{p}p$ annihilation into $\pi^+\pi^-$ and K^+K^- from the 2p state are $(4.81 \pm 0.49) \times 10^{-3}$ and $(2.87 \pm 0.51) \times 10^{-4}$ respectively. The pion yield is slightly larger than in liquid hydrogen, where $L=0$ annihilation dominates, while the kaon yield is suppressed by a factor of four. Using these and previous data, we derive the branching ratios for $\bar{p}p$ annihilation into all $\pi\pi$ and $K\bar{K}$ modes from S and P states. A measurement in gaseous hydrogen, without $X-$ray requirement, yields the branching ratios $(4.30 \pm 0.14) \times 10^{-3}$ and $(6.92 \pm 0.41) \times 10^{-4}$. With the known branching ratios of $(3.33 \pm 0.17) \times 10^{-3}$ and $(1.01 \pm 0.05) \times 10^{-3}$ in liquid hydrogen, we find that (50.3 ± 6.4) % of all annihilations in gas at NTP occur in the initial angular momentum state $L=1$.

1. INTRODUCTION

Antiprotons stopping in hydrogen are captured into the orbitals of antiprotonic hydrogen. In liquid hydrogen, $p\bar{p}$ annihilation from the s orbitals of the $\bar{p}p$ atom dominates. So far most available data stem from bubble chamber experiments [1]. Quantum number conservation therefore restricts our present knowledge of annihilation at rest, its dynamics and the production of intermediate meson resonances, to those channels accessible from $L = 0$ states. The contribution from higher partial waves can be studied at higher energies, albeit at the expense of complexity, since pure initial angular momenta cannot be prepared for annihilation in flight. We have therefore initiated a study of annihilation at rest from pure $L = 1$ states at the Low Energy Antiproton Ring (LEAR) at CERN, with the aim of contributing towards a more comprehensive understanding of the annihilation dynamics and production of intermediate resonances [2]. No such study has been previously performed.

Proton — antiproton annihilation at low energies is a suitable tool to study non perturbative quantum chromodynamics. As the proton and antiproton wavefunctions overlap, constituents quarks are expected to play an important role in the annihilation process. Several approaches to annihilation into two or three mesons have been proposed [3 − 11]. The process is interpreted as a rearrangement of the constituent quarks or as the annihilation and creation of $\bar{q}q$ pairs. For two meson final states, the main contributions stem from the annihilation of two $\bar{q}q$ pairs followed by the creation of a new pair (annihilation graph), or from the annihilation of one pair and rearrangement of the remaining four quarks (rearrangement graph). Two approaches based on SU(3) and on the quark line rule [12,13] predict the relative contributions of the two graphs to the annihilation branching ratios. The absolute branching ratios can also be predicted with further dynamical assumptions on the $\bar{q}q$ vertices. Some models [6,8,9] describe the $\bar{q}q$ vertices by the emission or absorption of single gluons ($^3S_1$ vertices) while others [3,5,7,11] prefer an effective $^3P_0$ coupling which can be understood as the emission or absorption of many gluons, an approach perhaps better suited to describe processes in the non perturbative regime of low energy annihilation. An essential ingredient of some of the models is in fact the initial angular momentum. In particular, the annihilation and rearrangement graphs contribute differently to S and P waves and could therefore be distinguished by measuring branching ratios for annihilation from S and P states.

The branching ratios for $\bar{p}p \rightarrow \pi^+\pi^-$ and K^+K^- have been measured in liquid hydrogen by several groups: the branching ratio for $\pi^+\pi^-$ is 0.32 ± 0.03 % for the Columbia group [14] and 0.37 ± 0.03 % for the CERN−Collège de France collaboration [1]. A recent counter experiment at LEAR reported 0.31 ± 0.03 % [15]. For K^+K^-, the corresponding figures are $(1.1\pm0.1)\times 10^{-3}$ [14], $(0.96\pm0.08)\times10^{-3}$, [1] and $(0.99\pm0.10)\times10^{-3}$ [15]. In liquid, C−parity conservation implies that the $\bar{p}p$ system annihilates from the $^3S_1$ state. The results presented here pertain to an investigation of $\bar{p}p$ annihilation at rest into $\pi^+\pi^-$ and K^+K^- from P states ($^3P_0$ and $^3P_2$) by using hydrogen gas at atmospheric pressure.

2. ANNIHILATION IN HYDROGEN GAS

Antiprotons stopping in hydrogen are captured in a high orbital ($n = 20$ to 40) of the antiprotonic atom. The $\bar{p}p$ system then collides with neighbouring H_2 molecules, whereby the electric field perturbation induces Stark transitions to the other angular momentum states of the same n orbital (Day−Snow−Sucher mechanism [16]). In dense gases or in liquid, the collision rate is so high that the system is more likely to reach the ns level than to radiate to lower orbitals. Once in the ns orbital, the system annihilates owing to the absence of angular momentum barrier. Thus $\bar{p}p$ annihilation in liquid hydrogen is dominated by annihilation with the initial angular momentum $L = 0$. The precise fraction of S wave in liquid is not well known. Bizzarri et al [17] quote a lower limit of 94% from a study of $K_S K_S$ and $K_S K_L$ in liquid hydrogen and deuterium.

In hydrogen gas at atmospheric pressure (NTP), the contribution of np orbitals to the annihilation is expected to increase due to the lower density and the correspondingly smaller collision rate. Furthermore, the electromagnetic cascade now develops down to the 2p level. From the observed small probability for a subsequent transition to the 1s level by emission of a K_α X−ray, one deduces that nearly all $\bar{p}p$ atoms annihilate from the 2p state (99 ± 1 %) [18 − 22]. The detection of the L X−rays in coincidence with the mesonic final states provides therefore a rather clean sample of P wave annihilation. We have measured the yield of the Balmer series (L X−rays to the 2p level) in hydrogen

gas at NTP: 13 ± 2% [21]. The energy range of the L X-rays lies between 1.7 keV (L_α) and 3.1 keV (L_∞).

This paper is organized as follows: after a description of the apparatus, we present results for $\bar{p}p \rightarrow \pi^+\pi^-$ and K^+K^- in hydrogen gas at NTP. The absolute branching ratios for P wave annihilation is then obtained for a subsample of the data with coincident L X-rays. We then comment on the fraction of P wave annihilation in gas and liquid, which can be determined from our data in conjunction with previous results. In the last section we derive the total $\pi\pi$ and $K\bar{K}$ rates from S and P waves and briefly compare our results with quark model predictions.

3. APPARATUS

The experiment was performed on the N2 beam line of the Low Energy Antiproton Ring (LEAR) at CERN. The apparatus is shown in fig. 1. Antiprotons of 105 MeV/c enter a solenoidal magnet of homogeneous field (0.8 T) along its symmetry axis. After passing through a 50μ thick scintillation counter T2, they stop in a hydrogen gas target at NTP (fig.2). A stopping $\bar{p}$ in hydrogen is defined by the coincidence T2$\bar{T}$3$\bar{T}$4.

The hydrogen gas is contained in an aluminized mylar cylinder, 6μ thick, 76 cm long and 16 cm diameter, transparent to X-rays with energies above 1 keV. The target is maintained at a slight overpressure of 1 Torr. The antiprotonic X-rays traverse the target membrane and are detected by conversion in an argon-ethane drift chamber (XDC) [23,24]. The signals are detected on 90 anode wires running parallel to the detector axis. The aluminized membrane is held at a high voltage of typically 10 kV. The drift space from the membrane to the signal wires is 6.4 cm which corresponds to a maximum drift time of 1.4 μs. The mean free path for L X-rays in a 50% argon, 50% ethane mixture increases with X-ray energy and varies between 1.6 and 7.8 cm. The drift time determines the conversion radius.

On each wire the pulse height is sampled every 32 ns by 6 bit flash ADCs and a time interpolator determines the drift time within 4 ns. This provides information on the slope and length of the pulses. Since X−ray conversions are localized in space, they can be distinguished from ionizing particles by their characteristic short pulses. The trajectories of the drift electrons are curved by the magnetic field, so that charged particles traverse several drift cells, usually firing four to five wires, while X−rays generate signals on isolated wires. This last feature can be used online to enhance events on tape that are associated with a detected X−ray: the "ONE GAP" condition requires one hit on at least one isolated XDC wire.

The coordinate z of the conversion point along the wire is determined by charge division of signals from both ends of the wire with an accuracy of $\sigma = 1.5$ cm. The chamber is calibrated with ^{57}Co and ^{54}Mn radioactive sources. The X−ray energy is determined from the integrated pulse height with a resolution of $\sigma = 0.26$ keV at 1.7 keV. The X−ray detection efficiency (including reconstruction efficiency) is typically 30% in the L X−ray region. Further details on the XDC can be found in ref. [23,24].

Charged annihilation products are detected by seven cylindrical multiwire proportional chambers (C_1, C_2, Q_1, Q_2, P_1, Q_3, P_2) with anode wires running parallel to the detector axis [25]. The wire spacing is typically 2 mm and the tracklength from C_1 to P_2, 68 cm. The C and Q chambers have cathode wires or strips providing the coordinates of the hits along the beam axis. The typical cathode wire spacing is 3 mm. The momentum resolution for pions of 928 Mev/c (eg pions from $\bar{p}p \rightarrow \pi^+\pi^-$) reaching P_2 is $\sigma = 49$ MeV/c for the data presented here, and is a linear function of momentum down to 300 MeV/c. For collinear events of the type $\pi^+\pi^-$ or K^+K^-, the resolution can however be improved by a factor of five by fitting one single track traversing the whole detector volume.

A stopping $\bar{p}$ is defined by the trigger $\overline{p}STOP = T2\overline{T}3\overline{T}4$. Since the solid angle covered by P_2 is 2π sr, many annihilation events have either missing tracks or tracks escaping the sensitive volume without reaching P_2. To enrich the data sample written to tape with fully reconstructable events of good momentum resolution, a multiplicity trigger can be used. A fast anode cluster counting is available on C_1, C_2, Q_2 and P_1 and is compared to a preset multiplicity. Two prong data were taken by

requiring at least three of the four chambers to have a cluster multiplicity of exactly two (trigger $\overline{p}STOP \times M$). This multiplicity trigger, when combined with the X-ray enhancing ONE GAP condition explained above, will be referred to as $\overline{p}STOP \times MX$.

For γ detection, the apparatus is supplemented by a lead converter inserted between P_1 and Q_3 and by two endcaps, each made of three planar hexagonal multiwire proportional chambers with a lead sheet inserted between the first and second chambers.

4. DATA REDUCTION

Data collected on tape (RDT) are analyzed by a trackfinder and the reconstructed tracks, X-ray and photon information written to data summary tape (DST). To appear on DST, an event is required to have at least one track, one X-ray or one photon. The fraction of lost events which do not lead to any DST information is 1%. The results presented here are derived from three DST data samples:

Two DST samples of respectively 1'005'312 (I) and 346'213 (II) $\overline{p}STOP$ events were collected during two different running periods. Although of poorer statistics, set (II) provides a useful consistency check of the results since the two sets were obtained under different experimental conditions (apparatus performance, chamber efficiencies, stopping distribution). We shall describe the data reduction for set (I) and merely quote results for set (II) since the analysis method is identical for both. Although the statistics are sufficient for $\pi^+\pi^-$, they are not adequate to determine accurately the rather small branching ratio for K^+K^- in coincidence with L X-rays. A third data sample (III) of 1'421'860 events collected with the $\overline{p}STOP \times MX$ trigger is used instead to derive the K^+K^- branching ratio from the relative K^+K^- and $\pi^+\pi^-$ intensities. An absolute determination of both branching ratios from set (III) alone is hard due to uncertainties in the efficiency of the $\overline{p}STOP \times MX$ trigger. The trigger inefficiency does not however influence the relative rates of $\pi^+\pi^-$ and K^+K^- events.

We shall describe the data reduction leading to the branching ratios $B_g(\pi^+\pi^-)$ and $B_g(K^+K^-)$ in hydrogen gas from set (I). The branching ratio $B_X(\pi^+\pi^-)$ for $\pi^+\pi^-$ in coincidence with L X-ray

candidates is obtained from the subsample of those events associated with a reconstructed X−ray in the L region. The background in the X−ray sample (discussed in section 4.4) is then subtracted to yield the branching ratio $B_1(\pi^+\pi^-)$ from the 2p level. The branching ratio $B_X(K^+K^-)$ for K^+K^- in coincidence with L X−ray candidates is then determined from the ratio R_X of K^+K^- and $\pi^+\pi^-$ rates obtained from set (III) and $B_X(\pi^+\pi^-)$. The branching ratio $B_1(K^+K^-)$ from the 2p level is finally obtained by subtracting the background contribution to the X−ray spectrum.

4.1 $\pi^+\pi^-$ and K^+K^- in hydrogen gas

Figure 3 shows the vertex distribution in the hydrogen gas target, obtained with $\bar{p}$STOP events of set (I), along the beam direction (a) and as a function of radius (b). The width of the stopping distribution is 12.5 cm along the beam direction. The arrows show the positions of T2 and T4 and the mylar membrane. The fractions of $\bar{p}$ stopping beyond the membrane is less than 2.6 %. This fraction includes events with a badly reconstructed vertex and is therefore an upper limit. The inset in fig.3 shows that the fraction of $\bar{p}$ stopping in and before T2 and in T4 is negligible (2×10^{-3}). Note that the annihilation point cannot be determined for events of the type $\pi^+\pi^-$ or K^+K^-, since no vertex is available.

The momentum distribution of two prong events from data set (I) is shown in fig. 4. For $\pi^+\pi^-$ and K^+K^-, the mesons are emitted back to back. Define

$$ t = (p_z/p_\perp)_1 + (p_z/p_\perp)_2 $$

where p_z ($p_\perp$) are the momenta parallel (perpendicular) to the magnetic field axis. Collinear events are expected to cluster around small values of $|t|$ as shown in the inset of fig.4. Events for which both tracks have a momentum of at least 500 MeV/c and for which $|t| < 0.1$ are selected. These events appear as single circular tracks in the transverse plane, traversing the whole detector. They are therefore submitted to a global circle fit in the transverse plane, yielding the perpendicular momentum with improved resolution [26]. The cylindrical surface containing the helicoidal trajectory is then developed

and a global straight line fit yields the parallel momentum. The distribution of the modulus of the fitted momentum, for those events satisfying the fits with a confidence level of more than 1% is shown in fig. 5. The K^+K^- and $\pi^+\pi^-$ peaks appear clearly with very small background. One finds $N = 2328$ pion and 348 kaon events in the momentum ranges [894,960] and [768, 828] MeV/c. A Gaussian fit yields the central values 924.9 ± 0.3 and 795.1 ± 0.7 MeV/c compared to the expected 927.8 and 797.9 MeV/c. The discrepancy of 3×10^{-3} could be due to the uncertainty in the magnetic field strength. The momentum resolutions are $\sigma = 13.1$ and 11.6 MeV/c respectively.

The detection and reconstruction efficiency η (which includes the solid angle acceptance) is calculated by Monte Carlo simulation of $\pi^+\pi^-$ and K^+K^- events using the stop distribution of fig.3 and the measured chamber efficiencies. The detection efficiencies η and their statistical errors are given in Table 1 (column 3). In addition, a systematical error of ± 2 % is due to uncertainties in the chamber efficiencies. The lower figure for the K^+K^- efficiency stems from kaon decay in the detector. The simulated data set is submitted to the same analysis chain. The momentum resolutions of the pion and kaon peaks are 12.2 and 11.3 MeV/c in agreement with real data. The raw branching ratios B computed from the number of $\pi(K)$ events, the number of DST events and the efficiencies are shown in column 4 of Table 1.

The branching ratios must be corrected for background annihilation channels. The main contribution stems from $\bar{p}p \rightarrow \pi^+\pi^-\pi^0$ events with collinear pions which generate background mainly under the kaon peak. This background is estimated by Monte Carlo simulation of the channel $\bar{p}p \rightarrow \pi^+\pi^-\pi^0$, assuming phase space distribution and the same branching ratio of 7% as in $\bar{p}p$ annihilation in liquid [1]. The contribution from the channel $\bar{p}p \rightarrow \pi^+\pi^-\pi^0\pi^0$ is at least one order of magnitude smaller and has been estimated with the same method using a branching ratio of 9 % [27]. Contributions from channels with higher π^0 multiplicities are negligible. In addition, the pion peak contributes a small background under the kaon peak. This correction is estimated by Monte Carlo using the branching ratios of column 4 (Table 1).

The correction b to the branching ratio B is given by

$$b = (\Sigma \; \eta_i B_i) \; / \; \eta$$

where η_i is the detection and reconstruction probability of a background event from channel i with branching ratio B_i. The efficiency η_i is calculated by Monte Carlo simulation. The corrections b (column 5) are small. The predicted background in the control regions around the peaks is in good agreement with the observed background.

The final results are given in column 6. Table 1 also shows the results obtained from data set (II). Taking the weighted mean of sets (I) and (II), one obtains the final results for $\bar{p}p$ annihilation in gas at NTP:

$$B_g(\pi^+\pi^-) \;=\; (4.30 \pm 0.10\,[\text{stat}] \pm 0.11\,[\text{syst}]) \times 10^{-3}$$

$$B_g(K^+K^-) \;=\; (6.92 \pm 0.37\,[\text{stat}] \pm 0.17\,[\text{syst}]) \times 10^{-4}.$$

The systematical error includes the systematical uncertainties in the efficiency η ($\pm 2\%$), in the number of $\bar{p}$ stops in hydrogen ($\pm 1.3\%$) and in the number of lost events on DST ($\pm 0.5\%$). The ratio of branching ratios is

$$R_g \;=\; B_g(K^+K^-)/B_g(\pi^+\pi^-) \;=\; (16.1 \pm 0.9\,[\text{stat}]) \%$$

and the systematical error cancels out.

4.2 $\pi^+\pi^-$ in coincidence with L X−ray candidates

For data set (I) a reduced sample of only 765'366 $\bar{p}$STOP events were found to be useful when searching for coincident X−rays. An X−ray is identified by requiring an isolated anode signal with no hit on the two preceeding and following adjacent anode wires. This cut eliminates most of the background from charged tracks. In addition the pulse shape determined from the first six 32 ns time bins has to be consistent with the fast decaying signal expected for a localized charge deposition. Finally, the coordinate along the beam axis is required to lie within ± 30 cm of the target center. Figure 6 shows the resulting energy distribution of the XDC pulses. The broad enhancement between below 4 keV is due to the unresolved L series with a small argon fluorescence contribution around 3 keV. The

long tail beyond 4 keV stems from bremsstrahlung. The fluorescence and bremsstrahlung backgrounds are discussed in section 4.4.

In the reduced data sample (I), 37′550 $\bar{p}$STOP events are associated with an X−ray in the range 1.3 to 4 keV. Events with two particles of opposite charge, each with more than 500 MeV/c, and with $|t| < 0.1$ are then selected. The global fit leaves 115 $\pi^+\pi^-$ and 6 K^+K^- events in the momentum ranges [894,960] and [768,828] MeV/c respectively. The absolute branching ratios $B_X(\pi^+\pi^-)$ and $B_X(K^+K^-)$ for collinear events in coincidence with L X−ray candidates are now obtained by using the reconstruction efficiencies η discussed in section 4.1 (see Table 1). However, since X−rays can be masked in the vicinity of ionizing tracks, the X−ray detection efficiency decreases with increasing charge multiplicity. The data sample associated with X−rays is therefore biased towards low multiplicities. A correction factor m (given in Table 2) has been applied. The larger correction for data set (I) is due to a few dead XDC wires during that running period. The resulting branching ratio (column 5) must still be corrected for background channels as discussed in the previous section. Table 2 also shows the results for set (II). Taking the weighted means of column 6 one finds

$$B_X(\pi^+\pi^-) = (4.69 \pm 0.37\,[\text{stat}] \pm 0.12\,[\text{syst}]) \times 10^{-3}.$$

Table 2 also gives the preliminary branching ratio

$$B_X(K^+K^-) = (3.18 \pm 1.12\,[\text{stat}] \pm 0.08\,[\text{syst}]) \times 10^{-4}.$$

4.3 K^+K^- in coincidence with L X−ray candidates

Data set (III) was collected with the $\bar{p}$STOP×MX trigger during the same running period as set (I). The same selection procedure for collinear events in coincidence with L X−ray candidates is used as in section 4.2. This leads to 4338 $\pi^+\pi^-$ and 289 K^+K^- events, the momentum distribution of which is shown in fig.7. A precise determination of the absolute branching ratios of both final states is not possible with set (III) alone due to uncertainties in the efficiencies of the multiplicity and ONE GAP

triggers. The relative rates of $\pi^+\pi^-$ and K^+K^- events in set (III) is however not biased by trigger inefficiencies, so that $B_x(K^+K^-)$ can be derived from $B_x(\pi^+\pi^-)$ and from the ratio

$$R_x = (N_K/N_\pi)(\eta_\pi/\eta_K)$$

where N_K and N_π are the background corrected rates and $(\eta_\pi/\eta_K) = 1.24\pm0.04$, the relative detection and reconstruction efficiency determined by Monte Carlo simulation of the $\overline{p}STOP \times MX$ trigger. Note that R_x does not depend on the absolute efficiencies η_π and η_K, but only on their ratio. The background corrected rates are

$$N_k = N/[1 + b_K/B_x(K^+K^-)]$$

with $N = 289$ and

$$N_\pi = N/[1 + b_\pi/B_x(\pi^+\pi^-)]$$

with $N = 4338$. The corrections $b_K = (4.92\pm0.48)\times10^{-5}$ and $b_\pi = (2.57\pm0.32)\times10^{-5}$ are obtained as described in section 4.1 by Monte Carlo simulation of the trigger $\overline{p}STOP \times MX$ for background events. The corrections are small and therefore not sensitive to the uncertainties in the trigger efficiency. In fact, the observed and predicted background above and below the peaks are in excellent agreement. Taking $B_x(K^+K^-)$ and $B_x(\pi^+\pi^-)$ from section 4.2 one finds $R_x = (7.21 \pm 0.66\ [\text{stat}])\ \%$. The branching ratio for K^+K^- in coincidence with L X−ray candidates is then

$$B_x(K^+K^-) = R_x \times B_x(\pi^+\pi^-)$$

$$= (3.38 \pm 0.41\ [\text{stat}] \pm 0.08\ [\text{syst}]) \times 10^{-4}.$$

4.4 X−ray background

The main background contribution to the X−ray spectrum stems from bremsstrahlung due to the sudden acceleration of charge in $\bar{p}p$ annihilation at rest [28,29], and from argon fluorescence around 3 keV. The bremsstrahlung contribution has been calculated with a sample of $\overline{p}STOP \times M$ events (without ONE GAP condition) [30]. Collinear $\pi^+\pi^-$ events were selected according to the analysis procedure described in section 4.1. The bremsstrahlung contribution to the X−ray spectrum was simulated by using all measured pion momenta and was compared to the observed coincident X−ray distribution. Fig. 8 shows the X−ray spectrum for $\pi^+\pi^-$ events together with the predicted bremsstrahlung distribution (curve). The calculation shows that the continuum above 4 keV is due to bremsstrahlung. The expected 1/E behaviour of the bremsstrahlung contribution is compensated below 1 keV by absorption in the mylar membrane of the XDC. The dip and peak structure around 3.0 keV is due to the K absorption edge of argon. The fractional bremsstrahlung contribution to the X−ray spectrum between 1.3 and 4 keV is found to be (14.8 ± 1.0) %.

A similar calculation for K^+K^- events leads to (19.4 ± 4.4) %. Note that the background contribution is larger for K^+K^- notwithstanding the smaller bremsstrahlung yield for the slower kaons. This is due to the suppression of the channel K^+K^- from P waves.

The yield of fluorescence quanta was estimated with cosmic rays traversing the XDC and found to be (1.4 ± 0.4) × 10^{-3} per minimum ionizing particle. The fractional contribution to the X−ray spectrum between 1.3 and 4 keV is then calculated from the number of $\pi^+\pi^-$ and K^+K^- events in the $\overline{p}STOP \times M$ sample: (6.1 ± 1.5) and (15.0 ± 5.8) %.

The total contribution of bremsstrahlung and fluorescence is then

$$G(\pi^+\pi^-) \quad = \quad (20.9 \pm 1.8) \ \%$$

$$G(K^+K^-) \quad = \quad (34.4 \pm 7.3) \ \% \ .$$

4.5 Annihilation from the 2p state

The $\pi^+\pi^-$ and K^+K^- yields for the fraction G of events in coincidence with bremsstrahlung and fluorescence X—rays is determined by the branching ratio B_g in gas. The fraction P of events associated with L X—rays in the X—ray coincidence samples of section 4.2 and 4.3 is

$$P = (1 - G) / (1 + \alpha)$$

where $\alpha = 0.8$ % is the fraction of S wave annihilation due to the 2p to 1s transition [18]. The branching ratio B_1 for $\overline{p}p$ annihilation from the 2p orbital is obtained from the relation

$$B_x = PB_1 + \alpha PB_0 + GB_g$$

where B_0 is the branching ratio from S states which we shall assume to be equal to the branching ratio B_ℓ in liquid. This assumption is rather good given the smallness of the correction αPB_0. Taking for B_ℓ the average of the results reported in ref. [1,14,15], $B_\ell(\pi^+\pi^-) = (3.33 \pm 0.17) \times 10^{-3}$, and adding all systematical errors in quadrature, one gets the final result

$$B_1(\pi^+\pi^-) = (4.81 \pm 0.49) \times 10^{-3}.$$

The corresponding calculation for K^+K^- does not lead to a meaningful result due to the large correction $G(K^+K^-)$ and the larger errors. Using instead

$$B_1(K^+K^-) = B_1(\pi^+\pi^-) R_x [1 - G(K^+K^-)] / [1 - G(\pi^+\pi^-)]$$

we find

$$B_1(K^+K^-) = (2.87 \pm 0.51) \times 10^{-4}$$

and the ratio

$$R_1 = B_1(K^+K^-)/B_1(\pi^+\pi^-) = (6.0 \pm 1.2) \%.$$

5. P/S RATIO IN LIQUID AND GAS

The fraction f(liq) of P wave annihilation in liquid can be calculated from $B_1(\pi^+\pi^-)$ and from the branching ratio $B(liq)(\pi^0\pi^0)$ in liquid. The channel $\bar{p}p \rightarrow \pi^0\pi^0$ is forbidden from s orbitals owing to Bose – Einstein statistics and parity conservation. Including the isospin factor we have

$$B(liq)(\pi^0\pi^0) = 1/2 \, f(liq) \, B_1(\pi^+\pi^-).$$

The branching ratio $B(liq)(\pi^0\pi^0)$ has been measured by three groups: $(4.8\pm1.0)\times10^{-4}$ [31], $(2.06\pm0.14)\times10^{-4}$ [32] and $(1.4\pm0.3)\times10^{-4}$ [33]. The first figure gives with our result for $B_1(\pi^+\pi^-)$ f(liq) = (20.0 ± 4.6) %, in disagreement with the 6 % upper limit of ref.[17]. Using the more precise value [32] one finds f(liq) = (8.6 ± 1.1) %. We emphasize that this result for f(liq) rests on the somewhat arbitrary choice for the measured $\pi^0\pi^0$ yield. The following conclusions are however rather insensitive to the P wave contamination in liquid, as long as f(liq) remains small, as indicated by the 6% upper limit of Bizzarri et al [17].

The branching ratios B_ℓ in liquid can now be corrected for P wave contamination. For S states,

$$B_0 = [B_\ell - f(liq)B_1] \, / \, [1 - f(liq)]$$

so that $B_0(\pi^+\pi^-) = (3.19 \pm 0.20) \times 10^{-3}$ and $B_0(K^+K^-) = (1.08 \pm 0.05) \times 10^{-3}$, using for B_ℓ the averages of the results reported in ref. [1,14,15].

The fraction f(gas) of P wave annihilation in gas can also be obtained:

$$f(gas) = (B_g - B_0) \, / \, (B_1 - B_0).$$

One finds (68.5 ± 23.7) % from the branching ratios for $\pi^+\pi^-$ and (48.8 ± 6.7) % from K^+K^-, leading to a weighted mean of (50.3 ± 6.4) %. This result is in excellent agreement with the fraction of P wave deduced from a measurement of the $K_S K_L$ branching ratio in gas [34] and in liquid [1], a process allowed from s orbitals, but forbidden from atomic p states: f(gas) = (54 ± 10) %.

6. DISCUSSION

Table 3 summarizes the branching ratios obtained so far. The ratio $R_0 = B_0(K^+K^-)/B_0(\pi^+\pi^-) = 0.34 \pm 0.03$ for S wave is much higher than the corresponding $R_1 = 0.060 \pm 0.012$ for P wave annihilation. This is due to the suppression of the annihilation channel $\bar{p}p \to K^+K^-$ by a factor of four when switching from S to P waves and, to a lesser extent, to the slight increase of the branching ratio for $\bar{p}p \to \pi^+\pi^-$.

The channel $\bar{p}p \to K^0\bar{K}^0$ is also suppressed from P waves. The $K^0\bar{K}^0$ system decays as $K_SK_S + K_LK_L$ from P states with the branching ratio $(8.2 \pm 1.3) \times 10^{-5}$ reported earlier by this collaboration [34]. It decays as K_SK_L from S states with the branching ratio in liquid [1] corrected for P wave contamination: $(8.5 \pm 0.5) \times 10^{-4}$.

The transition amplitude for $\bar{p}p \to K^+K^-$ or $K^0\bar{K}^0$ is a mixture of isospin 0 and 1 amplitudes:

$$A(K^+K^-) = (A_0 - A_1) / \sqrt{2}$$
$$A(K^0\bar{K}^0) = (A_0 + A_1) / \sqrt{2}.$$

One then arrives at the total (K^+K^- and $K^0\bar{K}^0$) branching ratio from S states

$$B_0(K\bar{K}) = (1.93 \pm 0.07) \times 10^{-3} = |A_0(S)|^2 + |A_1(S)|^2,$$

whereas from P states

$$B_1(K\bar{K}) = (3.69 \pm 0.53) \times 10^{-4} = |A_0(P)|^2 + |A_1(P)|^2.$$

The difference of K^+K^- and $K^0\bar{K}^0$ rates yields the interference terms

$$2\,\text{Re}\,A_0(S)^*A_1(S) = -(2.3 \pm 0.7) \times 10^{-4}$$
$$2\,\text{Re}\,A_0(P)^*A_1(P) = -(2.1 \pm 0.5) \times 10^{-4}.$$

In contrast, the dipion is a pure isospin state ($I = 0$ for P states and $I = 1$ for S states). For S states

$$B_0(\pi\pi) = B_0(\pi^+\pi^-) = (3.19 \pm 0.20) \times 10^{-3}$$

whereas for P states

$$B_1(\pi\pi) \ = \ 3/2 \ B_1(\pi^+\pi^-) \ = \ (7.22 \pm 0.73) \times 10^{-3}.$$

The above results may be summarized as follows:

1. The channel $\pi\pi$ is enhanced by a factor of 2.3 ± 0.3 when switching from S to P waves ($I = 1$ to $I = 0$).

2. The channel $K\bar{K}$ is suppressed by a factor of 5.2 ± 0.8 when going from S to P waves (for K^+K^- the factor is 3.8 ± 0.7 and for $K^0\bar{K}^0$, 10.4 ± 1.8).

3. The inequality of $B_1(K^+K^-)$ and $B_1(K^0\bar{K}^0)$ shows that both isospins $I = 0$ and $I = 1$ contribute without either being clearly predominant in P states. A negative interference between the two isospin states is observed with a magnitude close to the total $K\bar{K}$ rate.

4. Although the near equality of $B_0(K^+K^-)$ and $B_0(K^0\bar{K}^0)$ does not allow to make a clear statement about the relative isospin contribution to S states, the isospin interference term has a small negative value with a statistical significance of about 3σ.

It has been noticed earlier that the $K\bar{K}$ suppression from P waves cannot readily be explained by meson exchange models [35]. Several quark models predict however the $K\bar{K}$ suppression from P waves. A simple argument suggests why $K\bar{K}$ should be suppressed in the $^3P_0$ model: the annihilation graph is suppressed since for initial P wave the created $s\bar{s}$ pair must be in an even angular momentum state ($\ell = 0, 2$) owing to parity conservation. This is forbidden by the $^3P_0$ assumption ($\ell = 1$). Since the rearrangement graph does not contribute to $K\bar{K}$, the process is suppressed. Initial state scattering is however not included in this scheme and in fact, the suppression is also predicted by $^3S_1$ models when initial $\bar{p}p$ distortions are taken into account, as demonstrated by Kohno and Weise [8] for $\bar{p}p$ annihilation at 100 MeV/c. Oades et al. [36] extrapolate the helicity amplitudes obtained from [8] down to threshold and compute the partial widths for $\pi^+\pi^-$ and K^+K^-. The total annihilation width is taken from the imaginary part of the $\bar{p}p$ potential. The calculated $B_0(\pi^+\pi^-) = 3.3 \times 10^{-3}$ and

$B_1(K^+K^-) = 2.2 \times 10^{-4}$ are in excellent agreement with the experimental data while $B_0(K^+K^-) = 2.1 \times 10^{-3}$ agrees within a factor of two. The predicted branching ratio $B_1(\pi^+\pi^-) = 0.08$ exceeds however the experimental one by an order of magnitude, indicating that the helicity amplitudes for $\pi^+\pi^-$ extracted from [8] may be overestimated. Indeed, an extrapolation based on $N\bar{N} \rightarrow \pi\pi$ phase shifts yields $B_1(\pi^+\pi^-) = 0.01$, in fairer agreement with the experimental value (see ref. [36]).

Hartmann, Klempt and Körner [12] describe $\bar{p}p$ annihilation into two mesons by SU(3) invariant amplitudes. A quantitative calculation taking into account breaking of SU(3) by phase space and overlap of the $\bar{p}p$ and mesonic wave functions was presented in ref. [37]. In this model most data on $\bar{p}p$ annihilation at rest into two mesons can be reproduced with three parameters. For annihilation from P states into $\pi^+\pi^-$ and K^+K^- the model predicts $B_1(K^+K^-)/B_1(\pi^+\pi^-) = 0.036$ in fair agreement with our result. Significant distortions of the $\bar{p}p$ wave function by $n\bar{n}$ admixture would however change this prediction.

In summary, several models predict the observed $K\bar{K}$ suppression from P waves. Additional branching ratios for P wave annihilation will however be required to distinguish between models.

7. SUMMARY

The branching ratios for $\bar{p}p \rightarrow \pi^+\pi^-$ and K^+K^- at rest have been obtained in a pure angular momentum state $L(\bar{p}p) = 1$ using the novel technique of triggering on the Balmer series of the $\bar{p}p$ atom. While the $\pi^+\pi^-$ branching ratio increases slightly from $L = 0$ to $L = 1$, the K^+K^- process is suppressed from $L = 1$ by a factor of four. Using data for $\pi^+\pi^-$, $\pi^0\pi^0$, K^+K^- and $K^0\bar{K}^0$ in liquid and in gas, we have extracted all branching ratios for $\pi\pi$ and $K\bar{K}$ from both S and P waves. Annihilation into $K\bar{K}$ is suppressed from P waves as predicted by several quark models of $\bar{p}p$ annihilation.

Our data are consistent with a small ($\simeq 8\%$) P wave contribution to $\bar{p}p$ annihilation in the liquid hydrogen targets of previous experiments. P wave annihilation increases however to 50 % in hydrogen gas targets at NTP.

ACKNOWLEDGEMENTS

REFERENCES

[1] R.Armenteros and B.French, High Energy Physics, Vol. IV, ed. E.H.S.Burhop Academic, London (1969) 284.

[2] R.Armenteros et al., CERN proposal P28/PS171 (1980).

[3] C.B.Dover and P.M.Fishbane, Nucl.Phys. B244 (1984) 349.

[4] S.Furui, A.Faessler and S.B. Khadkikar, Nucl. Phys. A424 (1984) 495.

[5] A.M.Green and J.A.Niskanen, Nucl. Phys. A430 (1984) 605.

[6] M.Maruyama and T.Ueda, Progr. Theor. Phys. 73 (1985) 1211.

[7] N.Isgur and J.Paton, Phys. Rev. D31 (1985) 2910.

[8] M.Kohno and W.Weise, Nucl. Phys. A454 (1986) 429.

[9] E.M.Henley, T.Oka and J.Vergados, Phys. Letters 166B (1986) 274.

[10] M.Maruyama, S.Furui and A.Faessler, Nucl. Phys. A472 (1987) 643.

[11] M.Maruyama, S.Furui, A.Faessler and R.Vinh Mau, Nucl. Phys. A473 (1987) 649.

[12] U.Hartmann, E.Klempt and J.Körner, Phys. Letters 155B (1985) 163.

[13] H. Genz, Phys. Rev. D28 (1983) 1094, ibid. D31 (1985) 1136.

[14] C. Baltay et al., Phys. Rev. Letters 15 (1965) 532.

[15] G.A.Smith, Proc. of the Workshop "The elementary structure of matter", Ed. Springer, Les Houches, France (1987).

[16] T.B.Day, G.A.Snow and J.Sucher, Phys. Rev. 118 (1960) 864.

[17] R.Bizzarri et al, Nucl. Phys. B69 (1974) 307.

[18] M.Ziegler, PhD Thesis, Universität Mainz (1987).

[19] L. Simons, Proc. IV LEAR Workshop, Ed. Harwood Acad. Publ., Villars, Switzerland (1987) p.703.

[20] C.A.Baker et al., submitted to Nucl. Phys. A.

[21] S.Ahmad et al., Phys. Letters 157B (1985) 333.

[22] M.Ziegler et al., Phys. Letters B, in print.

[23] U.Gastaldi et al., Nucl. Instr. Methods 176 (1980) 99.

[24] U.Gastaldi, Nucl. Instr. Methods, 157 (1978) 441, ibid. 188 (1981) 459.

[25] S.Ahmad et al., Nucl. Instr. Methods 217 (1983) 169.

[26] M. Botlo, PhD Thesis, Universität Wien (1987).

[27] G.Ghesquière, Symp. on Antinucleon Nucleon Interactions,

Liblice, CERN Yellow Report 74 − 18 (1974) p.436.

[28] R.Rückl and C.Zupancic, Phys. Letters 150B (1985) 225.

[29] U.Schaefer, PhD Thesis, Universität München (1987).

[30] M.Doser, PhD Thesis, Universität Zürich (1988).

[31] S.Devons et al., Phys. Rev. Letters 27 (1971) 1614.

[32] L.Adiels et al., Z. Phys. C35 (1987) 15.

[33] G.Bassompierre et al, Proc. 4th European Antiproton Symp., Barr, Vol I, (1978) p.139.

[34] S.Ahmad et al, Proc. III LEAR Workshop, ed. Frontières, Tignes,

France (1985) p.353.

[35] P. Christillin, Lett. Nuov. Cim. 41 (1984) 133.

[36] G.C. Oades et al., Nucl. Phys. A464 (1987) 538.

[37] E. Klempt, Proc. IV LEAR Workshop, Ed. Harwood Acad. Publ.,

Villars, Switzerland (1987) p.429.

Table captions

Table 1   Branching ratio B_g in gas for $\pi^+\pi^-$ and K^+K^-

(statistical errors only). n − data sample,

N − number of collinear events, η − detection efficiency,

B − raw branching ratio, b − background.

Table 2   Branching ratio B_x in gas for $\pi^+\pi^-$ and K^+K^- in

coincidence with L X−ray candidates (statistical errors only).

n_x − data sample, N − number of collinear events,

η − detection efficiency, m − X−ray correction,

B − raw branching ratio. The background contribution is taken

from column 5 of Table 1.

Table 3   Summary of branching ratios: B_0 from S states, B_ℓ in

liquid, B_g in gas at NTP, B_1 from P states.

(All systematical errors have been added in quadrature).

Table 1

n 1	N 2	η 3	$B = N/n\eta$ 4	b 5	$B_g = B - b$ 6
set (I) 1'005'312	$\pi^+\pi^-$ 2328	0.548 ± 0.010	4.23 ± 0.12 10^{-3}	2.68 ± 0.29 10^{-5}	4.20 ± 0.12 10^{-3}
	K^+K^- 348	0.464 ± 0.010	7.46 ± 0.43 10^{-4}	5.15 ± 0.54 10^{-5}	6.95 ± 0.43 10^{-4}
set (II) 346'213	$\pi^+\pi^-$ 921	0.587 ± 0.011	4.53 ± 0.17 10^{-3}	2.51 ± 0.80 10^{-5}	4.51 ± 0.17 10^{-3}
	K^+K^- 127	0.483 ± 0.010	7.59 ± 0.69 10^{-4}	7.51 ± 1.14 10^{-5}	6.84 ± 0.70 10^{-4}

Table 2

n_x 1	N 2	η 3	m 4	$B = Nm/n_x\eta$ 5	$B_x = B - b$ 6
set (I) 37'550	$\pi^+\pi^-$ 115	0.548 ± 0.010	0.879	4.91 ± 0.47 10^{-3}	4.89 ± 0.47 10^{-3}
	K^+K^- 6	0.464 ± 0.010	0.879	3.03 ± 1.24 10^{-4}	2.51 ± 1.24 10^{-4}
set (II) 17'574	$\pi^+\pi^-$ 54	0.587 ± 0.011	0.839	4.39 ± 0.60 10^{-3}	4.37 ± 0.60 10^{-3}
	K^+K^- 7	0.483 ± 0.010	0.839	6.92 ± 2.62 10^{-4}	6.17 ± 2.62 10^{-4}

Table 3

	B_0	B_ℓ	B_g	B_1
$\pi^+\pi^-$	3.19 ± 0.20 10^{-3}	3.33 ± 0.17 10^{-3}	4.30 ± 0.14 10^{-3}	4.81 ± 0.49 10^{-3}
K^+K^-	1.08 ± 0.05 10^{-3}	1.01 ± 0.05 10^{-3}	6.92 ± 0.41 10^{-4}	2.87 ± 0.51 10^{-4}

Figure captions

Fig.1   Side and front views of the ASTERIX spectrometer.

   1 – H_2 gas target, 2 – X – ray drift chamber, 3 – lead converter,

   4 – cylindrical MWPC, 5 – coil, 6 – yoke, 7 – planar MWPC.

Fig.2   Gas target and X – ray Drift Chamber (XDC).

   1 – anode signal wires, 2 – field shaping wires,

   3 – mylar membrane, 4 – argon/ethane drift volume, 5 – H_2 gas target,

   T2 – beam defining counter, T3, T4 veto counters.

Fig.3   Vertex distribution in the hydrogen target along the beam axis (a)

   and radially (b). The expanded view (inset) shows the contribution

   from antiprotons stopping in T2.

Fig.4   Momentum distribution of two prong events in hydrogen gas

   (two entries per event). Distribution in t (inset) for events with

   both momenta > 500 MeV/c. The arrows show the cuts applied to

   select collinear events.

Fig.5   Momentum distribution for collinear events (one entry per

   event) after the global track fit.

Fig.6   X – ray energy spectrum.

Fig.7   Momentum distribution of collinear events in coincidence with

   X – rays in the range 1.3 to 4 keV.

Fig.8   X – ray energy spectrum for $\pi^+ \pi^-$ events. The

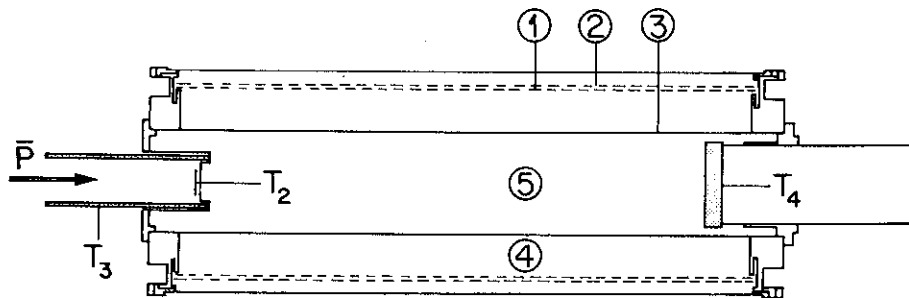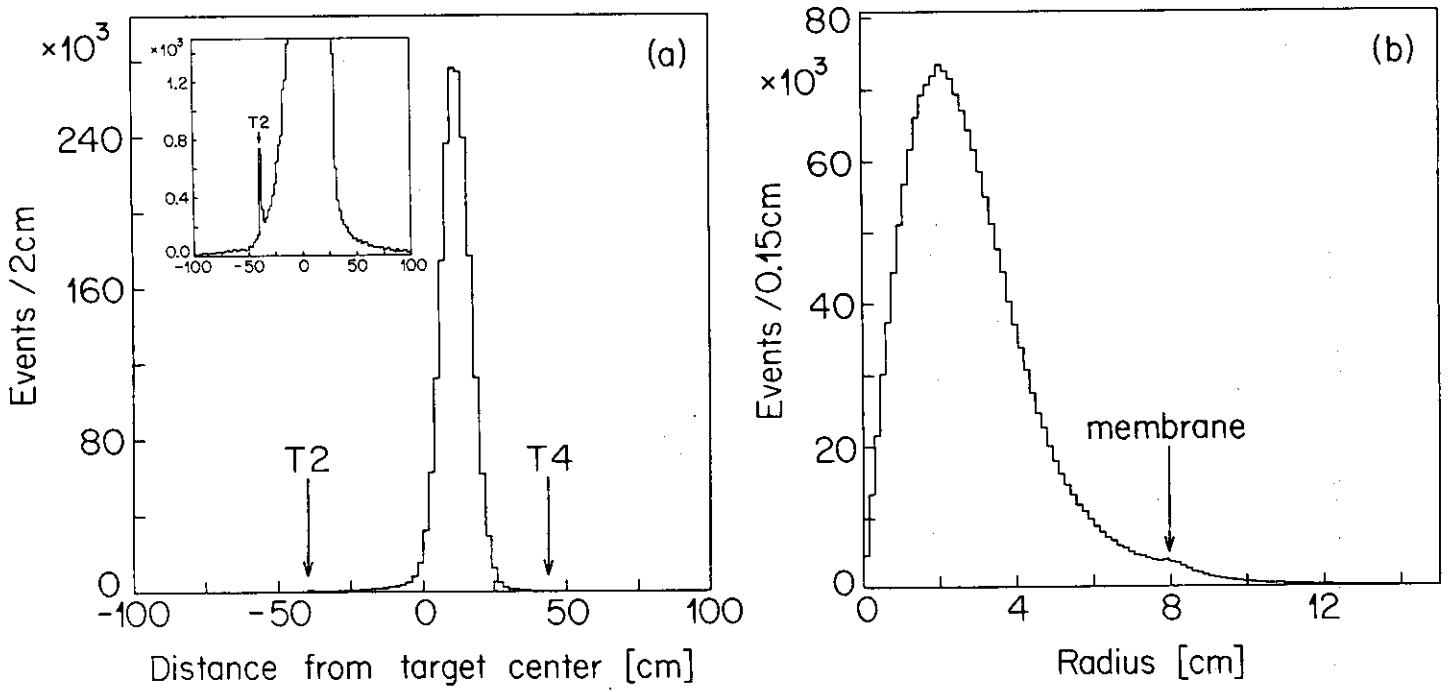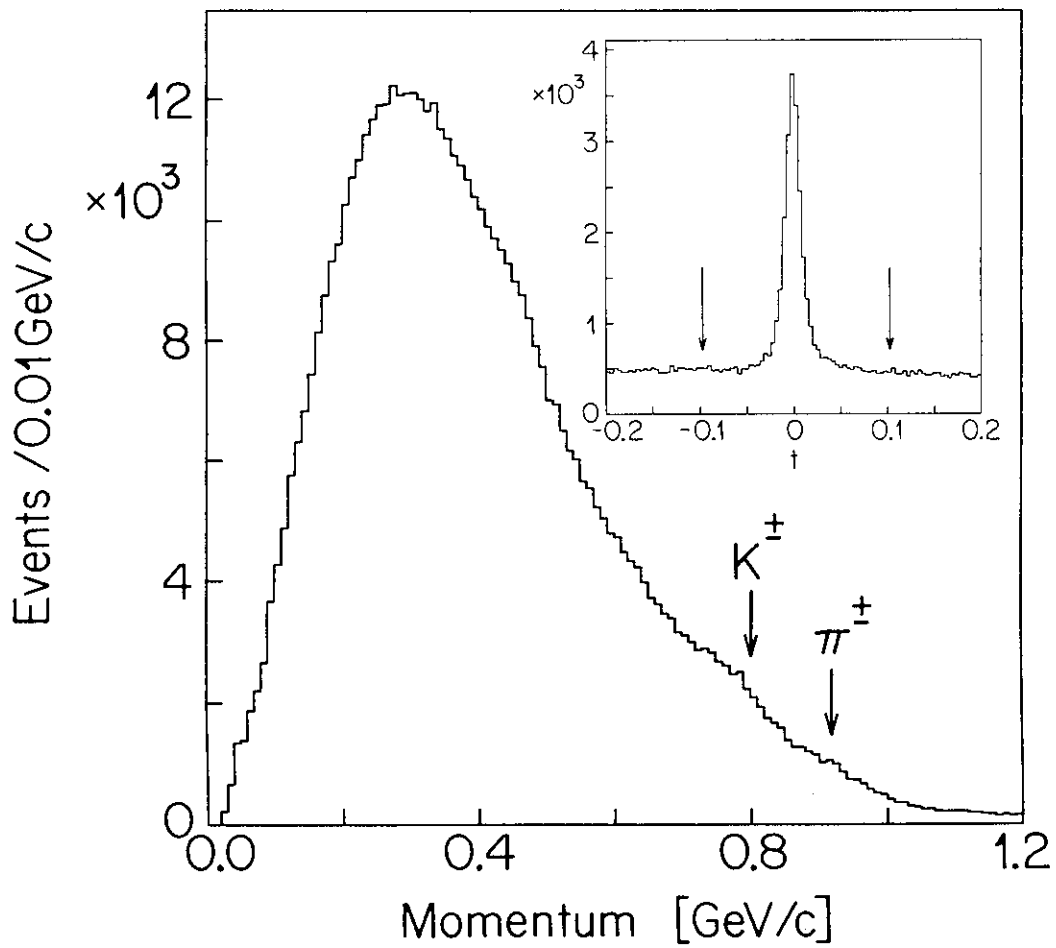   curve shows the calculated contribution from bremsstrahlung.
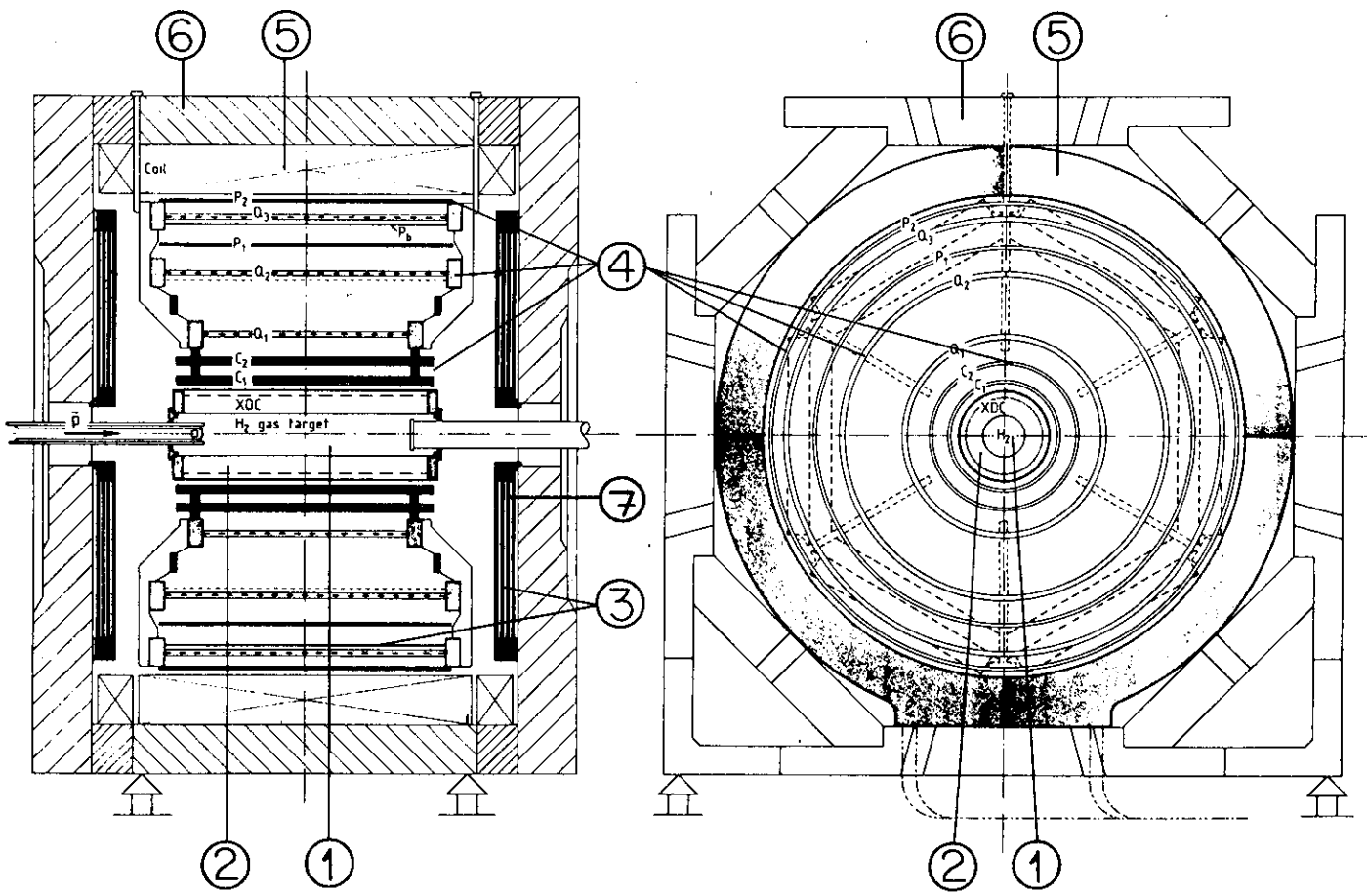
Fig.1

Fig.2

Fig.3

Fig.4

Fig.5

Fig.6

Fig.7

Fig.8